

Nanoscale depth-resolved polymer dynamics probed by the implantation of low energy muons

Francis L. Pratt ^{a,*}, Tom Lancaster ^{b,c}, Peter J. Baker ^{b,a}, Stephen J. Blundell ^b, Thomas Prokscha ^d, Elvezio Morenzoni ^d, Andreas Suter ^d and Hazel E. Assender ^e

^aISIS Facility, Rutherford Appleton Laboratory, Chilton, Oxfordshire OX11 0QX, United Kingdom

^bUniversity of Oxford, Department of Physics, Clarendon Laboratory, Parks Road, Oxford OX1 3PU, UK

^cCentre for Materials Physics, Department of Physics, Durham University, Durham DH1 3LE

^dPaul Scherrer Institut, CH-5232 Villigen PSI, Switzerland

^eUniversity of Oxford, Department of Materials, Parks Road, Oxford OX1 3PH, UK

Abstract

The low energy muon (LEM) technique has been used to probe local changes in the dynamical spectrum of thin film polymer samples taking place as a function of the temperature and the implantation depth below the free surface. The studies have been made on samples of polydimethylsiloxane (PDMS) and polybutadiene (PB) using the transverse magnetic field (TF) configuration and diamagnetic probe muons. In PDMS evidence is found for suppression of the glass transition temperature near the surface, along with significantly modified dynamics in the near-surface region as well as at depths significantly below the surface. For PB the LEM technique reveals well-defined layers of dynamical and spatial inhomogeneity at depths of order 0.1 to 0.2 μm below the free surface. These inhomogeneous regions may be assigned to nanopores produced by solvent streaming during preparation of spin-cast films. A thermal annealing procedure is shown to significantly reduce the thickness of these inhomogeneous layers. These results demonstrate that using LEM in the TF configuration provides a promising new method for studying surface-modified local dynamics of polymers that is also able to reveal nanostructured buried layers in polymer films.

Key words: Polymer surfaces, Surface dynamics, Surface phase transitions and critical phenomena, μSR

PACS: 68.47.Mn, 68.35.Ja, 68.35.Rh, 76.75.+i

1. Introduction

After the discovery of significant suppression of the glass transition temperature T_g for freestanding polystyrene (PS) films of nanoscale thickness [1], many detailed studies of thin polymer films have been made using a wide variety of techniques [2–4]. These results can be explained on the basis of a local T_g and associated local dynamics that varies

with the distance below a free surface [5], but there has previously been a lack of experimental techniques able to resolve such dependences in individual samples. Implanted low energy muons [6,7] provide a local probe technique that can be used to make nanoscale depth-resolved measurements mapping out the local dynamical properties and associated T_g in an individual polymer sample, which can be used to detect dynamical inhomogeneity and identify the mechanisms producing the reduced T_g near the free surface.

Our previous LEM study of PS used the zero field (ZF) configuration [10], where the relaxation

* Corresponding author.

Email address: francis.pratt@stfc.ac.uk (Francis L. Pratt).

is dominated by paramagnetic muoniated radical states [11,12] (the various types of muon probe state are discussed in detail in section 3). Evidence was found there for a significant suppression of T_g compared to the bulk value, with the region of suppressed T_g extending over a length scale of order 40 nm below the free surface. Recently Kanaya *et al.* made further LEM measurements on PS samples in the form of thin multilayer dPS/hPS films, measured using the longitudinal field (LF) configuration [13]. These results confirmed the presence of the reduction of T_g near the surface and provided good consistency with neutron reflectivity measurements made on the same samples [14].

In this report we present results on modified dynamics in the surface region of two further polymer systems PDMS and PB. We have studied the reduction in T_g in the near-surface region of PB and its dependence on molecular weight and these results are being reported elsewhere [15], in the present paper we reveal some interesting properties of PB films occurring at depths beyond the near-surface region that reflect buried layers that are significantly more inhomogeneous than the layers immediately above and below them. One of the features of these new studies on PDMS and PB is that we employ the TF configuration and the local dynamical probe is provided by muons in the so-called diamagnetic state, i.e. an environment without unpaired electronic spins. This is in contrast to the two earlier LEM reports on PS that used paramagnetic muoniated radicals as the probe states [10,13].

The paper is organised as follows. In section two the samples, the experimental technique and the data analysis methods are described. The nature of the probe states in these polymers and the coupling of the diamagnetic states to the local dynamics are then discussed in section three. Section four presents the main LEM experimental data for PDMS and PB. A final discussion and conclusion are presented in section five.

2. Experimental Details

2.1. Samples

The PDMS used in this study was obtained from two different suppliers and the samples are characterised by molecular weight M_w and molecular weight distribution defined by the polydispersity index $PDI = M_w/M_n$. Three samples were obtained

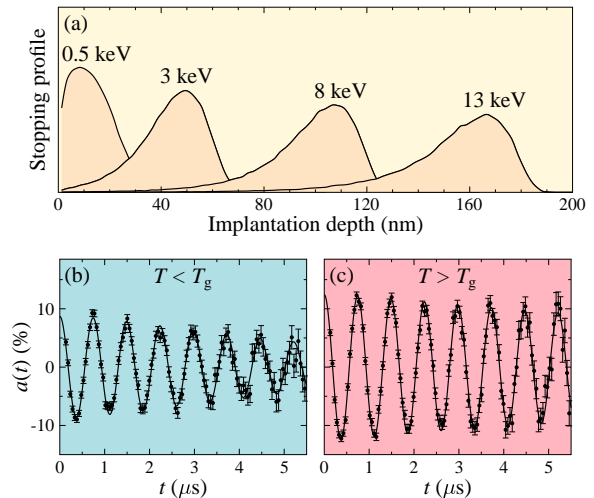


Fig. 1. (a) The muon stopping profile calculated using TRIM.SP for slow muons in PDMS with different implantation energies. (b) and (c) show the precessing positron asymmetry signals for PDMS in one pair of detectors at 100 K and 180 K, measured using 10 mT TF and 3 keV muons. Below T_g a significant damping of the signal is observed due to static nuclear dipolar fields in the glass state (b). Above T_g the damping is very weak due to motional averaging of the dipolar fields in the liquid state (c). Solid lines in (b) and (c) show fits to the TF Abragam function, from which the fluctuation rate ν of the local field may be derived as a function of temperature.

from Alfa Aesar ($M_w = 14$ kDa, 63 kDa and 139 kDa, $PDI = 1.7$) and two lower PDI samples were supplied by Polymer Source Inc. ($M_w = 33,500$, $PDI = 1.06$ and $M_w = 98,000$, $PDI = 1.4$). The PB samples used in these measurements had low PDI and were obtained from Polymer Source Inc. (1,4-addition, $M_w = 25.1$ kDa, $M_w / M_n = 1.01$ and $M_w = 95$ kDa, $M_w / M_n = 1.02$). Samples were prepared for the LEM measurements by casting a toluene solution on to silicon substrates using a spin coater rotating between 1600 and 2000 rpm. A typical resulting film thickness of $0.5 \mu\text{m}$ was estimated from ellipsometry of films prepared under identical conditions on glass substrates.

2.2. Instrument

The majority of the muon measurements were performed at the $S\mu$ S, Paul Scherrer Institut, Switzerland using the LEM instrument [6–9], additional bulk reference measurements were made using 3.7 MeV μ^+ surface muons using the GPS and DOLLY instruments at PSI and the ARGUS spectrometer at ISIS. The low energy muons are gener-

ated by moderation of the high intensity polarised beam of surface μ^+ using a thin film of Ar held at 10 K. Electrostatic elements are used to extract epithermal muons with energy ~ 15 eV and accelerate them up to 20 keV for transportation to the sample target where they are slowed down to provide a implantation energy that can be continuously varied from below 1 keV to values up to ~ 30 keV. In these experiments the implantation energy of the muons was varied between 0.49 keV and 23 keV by varying both the target and moderator potentials.

For the LEM measurements the initial spin polarization of the implanted muon was parallel to the plane of the film. A magnetic field was applied perpendicular to the plane of the film, i.e. perpendicular to the initial muon polarization giving a transverse field (TF) configuration in which diamagnetic muons precess at the frequency given by $\omega_\mu = \gamma_\mu B$ where $\gamma_\mu/(2\pi) = 13.55$ kHz/G and B is the applied field. The time evolution of the polarization of the muon ensemble was measured with four groups of positron emission detectors arranged in the TF precession plane. Using the Monte Carlo program TRIM.SP [16], which has been shown to accurately describe the stopping profile of slow muons [17], the range of the slow muons in PDMS was estimated for different implantation energies (Fig.1a). This shows that the mean depth being probed here by the muons is being tuned between 10 nm and 200 nm, a length scale over which the dynamical properties are expected to evolve between surface-dominated and bulk-dominated.

2.3. TF Data Analysis

TF- μ SR data were taken across the glass transition region by first cooling the sample to a temperature well below bulk T_g (e.g. 50 K or 100 K) and then taking data at a number of temperature steps on a warming sequence. The signal contribution from paramagnetic states in TF is at much higher frequency than the diamagnetic signal and is heavily damped, so it can easily be separated from the diamagnetic signal by analysing over an appropriate time range that excludes the earliest times. Data analysis was carried out using the program WiMDA [18]. The observed TF relaxation is due to the response of the muon to nuclear dipolar fields at the muon site, that originate from nearby protons in the polymer. At very low temperatures these fields will be static and the muon relaxes relatively fast

by coupling to these static fields (Fig.1b). At moderate temperatures within the glass phase there will also be a modest dynamic component due to fluctuations originating from local degrees of freedom of the polymer. Above the glass transition, the fluctuation rate of these local fields greatly increases, due to the onset of additional motional contributions, such as the α relaxation process, leading towards a motionally narrowed regime for the local field where the damping rate of the muon relaxation signal is greatly reduced (Fig.1c). This motional narrowing can be quantified by fitting the time dependence of the precessing asymmetry signal $a(t)$ to the form

$$a(t) = a_D \cos(\gamma_\mu B t + \phi) G_x(t) \quad (1)$$

where a_D is the diamagnetic asymmetry, B is the applied field, ϕ is the geometry-related detector phase and $G_x(t)$ is the Abragam transverse relaxation function [19] given by

$$G_x(t) = \exp(-\sigma^2 [e^{-\nu t} + \nu t - 1]/\nu^2) \quad (2)$$

where σ/γ_μ is the width of the field distribution in the static limit and ν is the temperature dependent fluctuation rate of the field in the dynamic regime. This Abragam function is well established in the field of nuclear magnetic resonance as a way to describe the crossover from slowly fluctuating local fields to fast fluctuating local fields and applies equally well to the TF μ SR configuration employed here. For slow fluctuations $G_x(t)$ takes a Gaussian form with relaxation rate σ whereas for a fluctuation rate ν that is fast compared to the timescale of the measurement the relaxation function $G_x(t)$ takes a Lorentzian form with relaxation rate σ^2/ν . All dynamical processes that modulate the position of the protons in relation to the muon will contribute to the effective value of ν , so there is not expected to be a simple direct scaling with the relaxation times obtained from other techniques, such as dielectric spectroscopy.

Two approaches to fitting the TF data were used. In the first method the static width parameter σ was allowed to vary with implantation depth and was determined at the lowest T in the scan (typically 50 K or 100 K) and then kept fixed for the analysis of the full T scan using Eqn.1. This simple method gives a T dependence of ν from which a good estimate of T_g can be obtained, but it was found to produce an anomalously large increase in σ as the surface was approached, which must reflect the residual background signal from reflected muons, rather than the dipolar width in the sample, which is not

expected to vary significantly with depth. A second fitting method was therefore used in which the sample width σ was not allowed to vary as implantation energy E is reduced and an E -dependent but T -independent background term was included, i.e.

$$a(t) = \cos(\gamma_\mu Bt + \phi)(a_D G_x(t) + a_{BG} G_{BG}(t)) \quad (3)$$

where the background term takes the Gaussian form $G_{BG}(t) = e^{-(\sigma_{BG}t)^2}$.

For the purposes of characterising the probe states in each sample some measurements were also made in LF mode. Here the detectors are arranged into two groups forward (F) and backward (B) with respect to the initial muon spin direction. The FB asymmetry signal a_{FB} is then defined in terms of the F and B signals as

$$a_{FB}(t) = (F(t) - \alpha_c B(t))/(F(t) + \alpha_c B(t)) \quad (4)$$

where α_c is a calibration factor reflecting the overall difference in the sensitivity of the F and B detector groups. A TF measurement made at low field with this detector grouping serves to both calibrate the FB asymmetry and also measure the amplitude of the diamagnetic fraction.

3. The Muon Probe States

The possible muon states in the polymers can be assigned to four categories (Fig.2) based on two defining characteristics. The first characteristic is whether the muon is free or is bound to the polymer. The second characteristic is whether the electronic nature of the state is open shell, labelled as ‘paramagnetic’, or closed shell, labeled as ‘diamagnetic’. Paramagnetic states are dominated by hyper-

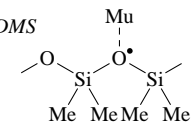
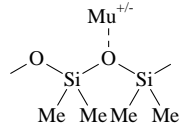
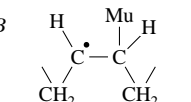
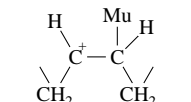
	Paramagnetic	Diamagnetic
Free	Mu [•]	Mu ^{+/-}
Bound	<p><i>PDMS</i></p> 	
	<p><i>PB</i></p> 	

Fig. 2. The four general classes of muon probe state for μ SR studies with the specific stable bound states shown for the PDMS and PB polymers investigated here.

	A MHz	D_1 MHz	D_2 MHz	A_p MHz	Q_A
PDMS (DFT) ^a	377	50	12	11	1.29 ^b
PB (DFT) ^c	345	30	5	95	1.14 ^d
PB (experiment) ^d	347(6)			74(3)	

Table 1

Hyperfine parameters calculated for the paramagnetic states in the two polymers studied here. The anisotropic hyperfine coupling is defined by the three parameters (A, D_1, D_2) where A is the isotropic part and the anisotropic dipolar part D is resolved into the main axial (D_1) element and a smaller and non-axial (D_2) element [20]. A_p is the largest proton coupling. Q_A is the quantum correction factor for A . ^aa segment of the form SiMe₃-O-SiMe₂-OMu-SiMe₂-SiMe₃ is used for the calculation. ^bthe experimental value of Q_A for the muoniated radical in benzene is assumed. ^ca cis-PB segment of 5 monomers is used for the calculation. ^dvalues from experiment [11] are extrapolated back to $T=0$ (see inset to Fig.4a) leading to the given estimate of the Q_A value.

fine coupling between the muon and the unpaired electron. The presence of such states is clearly revealed by the presence of a component of asymmetry that can be decoupled by a longitudinal magnetic field (Fig.3a, Fig.4a). The decoupling follows a series of broad steps with characteristic fields that are related to individual elements of the muon hyperfine tensor [20], i.e. the isotropic coupling A and the dipolar coupling D . The hyperfine coupling between the electronic spin and the protons A_p also contributes to the decoupling of the asymmetry in the low field region.

Density functional theory (DFT) allows a computational investigation to be made on the relative stability of such states and their expected hyperfine tensors. We have used DFT techniques optimised for state energetics and for hyperfine tensor evaluation. For evaluation of energetics, short polymer segments are sufficient, whereas hyperfine tensor calculations are more sensitive to extended spin delocalisation and require longer segments. In these calculations the semi-empirical Hartree-Fock method PM3 is first used for efficiently determining equilibrium geometries and then DFT with the B3LYP functional and the cc-pVDZ basis set is used for calculating the electronic properties including hyperfine tensors. The Gaussian package[22] was used for all the DFT calculations. This hybrid semi-empirical/DFT method for muoniated radical states has been developed and benchmarked against a range of experimental muon data [21]. Hyperfine parameters ob-

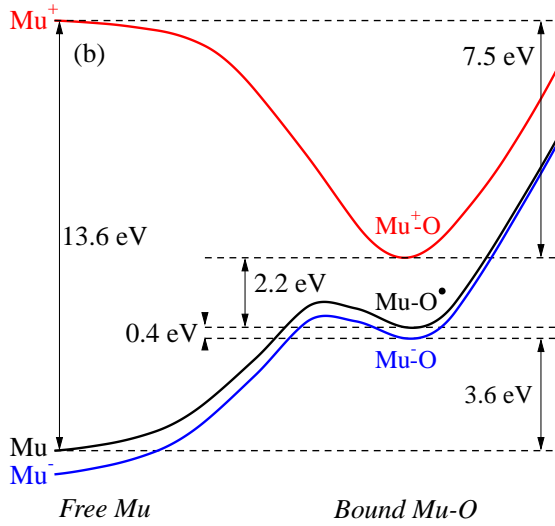
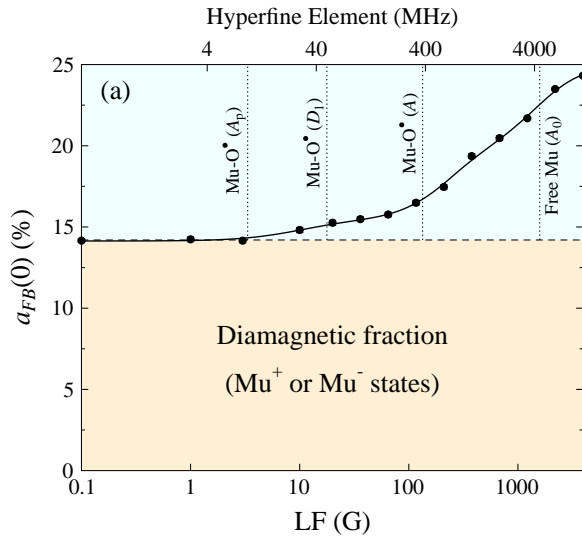


Fig. 3. (a) The LF repolarisation curve in PDMS plotting the initial FB asymmetry measured at 10 K. The paramagnetic fraction repolarises over a range of fields starting at the field expected from DFT calculations of the equilibrium state of the O-Mu radical and extending up to the characteristic repolarisation field of free muonium, which is characterised by isotropic hyperfine coupling $A_0 = 4464$ MHz. (b) Illustration of the energetics of the different muonium states in PDMS in free and bound form derived from DFT calculations on short polymer segments. The vertical axis is the energy scale and the horizontal axis represents a notional reaction coordinate. If mobile electrons are available then the radical can capture one of these to form the more stable bound Mu^- state, which is diamagnetic.

tained in this way are listed in Table 1.

For assessing the relative stability of the bound Mu^- states the larger basis set aug-cc-pVDZ is used, as calculation with this extended basis correctly de-

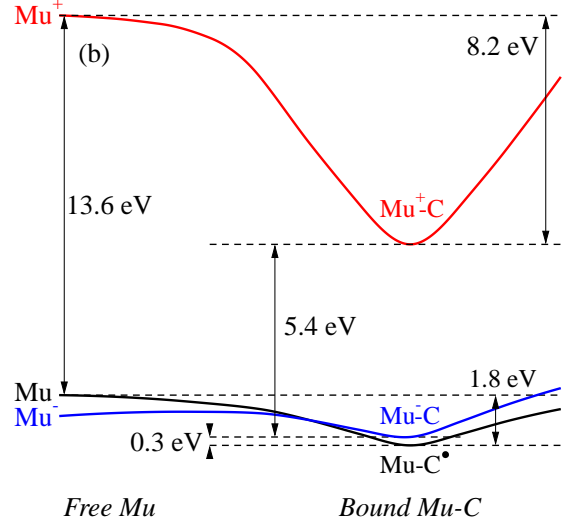
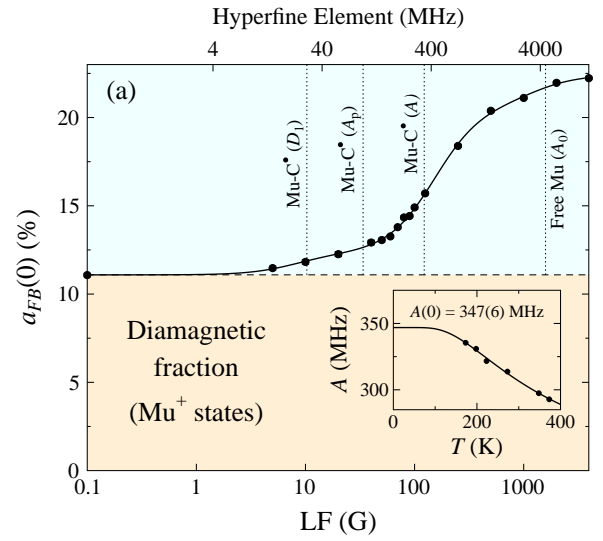


Fig. 4. (a) The LF repolarisation curve measured for PB at 11 K. The diamagnetic fraction is smaller than in PDMS. The inset shows a thermal excitation fit and corresponding $T=0$ value for A obtained from fitting to earlier PB data [11]. (b) Illustration of the relative energies of the muon states in PB. Note that in contrast to PDMS the bound Mu^- state is higher in energy than the radical state and is thus unstable with respect to losing one of its electrons to form the radical state.

termines the stability of the free H^- or Mu^- state with a reasonably accurate value for the electron affinity.

The energetics of the muon states in the two polymers is summarised in Fig.3b and Fig.4b. In both cases a free positive muon is found to form a bound state with the polymer, adding to the oxygen site in PDMS and to one of the unsaturated carbons in PB.

In the case of PB (Fig.4b), free muonium will re-

act with an unsaturated carbon to form the paramagnetic muoniated radical state [11]. This state can also be reached from the diamagnetic positive bound state by capture of a free electron (radiolytic free electrons are produced in the slowing down process of the muon). The diamagnetic negatively charged bound state that might form by capturing a second electron is not stable here against the single electron radical state. The diamagnetic state in PB is therefore assigned to the positive bound state and the paramagnetic state is assigned to the bound radical state with no significant free muonium fraction expected.

In contrast, for the case of PDMS (Fig.3b) there is a barrier against capture of free thermal muonium at the oxygen site, although an epithermal process may be possible. The most likely route to the paramagnetic radical state is therefore through electron capture by the positive bound state. In contrast to PB, the negative bound state is stable here compared to the neutral state, as it is in free muonium. The limited supply of radiolytic electrons will then determine the final balance between the three charge states of bound muonium. The diamagnetic fraction in PDMS (Fig.3a) is larger than in PB (Fig.4a) and this may reflect the additional possibility of negative diamagnetic states in PDMS, that is precluded in the case of PB.

The diamagnetic muons used as the probe states in the present study are therefore expected to be bound to the polymer rather than free. The muon spin relaxation rate for the diamagnetic states is relatively low with relaxation times on the order of many μs . For the diamagnetic signal the TF lineshape and corresponding relaxation function is determined by the average projection of the nuclear dipolar field at the muon site on the applied field direction. These dipolar fields originate from the protons in the polymer that are close to the muon site and produce a static contribution to the linewidth in the glass phase. The protons may be on the same element of the polymer as the muon (intrachain) or may be from adjacent polymer chains (interchain). Since the dipolar coupling follows the relative orientation of the muon-proton vector with respect to the field axis as $3\cos^2\theta - 1$, fast segmental reorientation will effectively average away the intrachain contribution to zero. The dynamical averaging of interchain contribution depends on the details of the chain interaction geometry within the fast dynamical state but fast interchain motion will also lead to a motional narrowing of the interchain contribution

to the line width and eventually this contribution will also average away to zero.

The significant diamagnetic fraction found in both polymers makes them well suited to being studied using the LEM technique in the TF configuration. The TF LEM results for the two polymers are now presented, looking first at changes in local dynamics near the surface in PDMS and then focusing on the dynamical behaviour in PB in regions at depths of 100 nm or more below the free surface.

4. Main Experimental Results

4.1. Data for PDMS

The fluctuation rate ν of the local field at the muon site obtained from analysing LEM measurements of PDMS in TF of 10 mT using Eqn.1 is shown for a range of implantation energies in Fig.5a-d. The glass transition temperature T_g is obtained from the data via the change in slope of the temperature dependence of ν versus T . The slope is defined as $\lambda = d\nu/dT$ with λ_g being the value in the glass state below T_g and λ_m the value in the melt above T_g . The solid lines in Fig.5 are fits to the function $\nu(T)$ defined in terms of two T linear regions

$$\nu(T) = \nu_0 + \lambda_g T \quad : \quad T < T_g, \quad (5)$$

$$\nu(T) = \nu_0 + \lambda_g T_g + \lambda_m (T - T_g) \quad : \quad T > T_g.$$

From Fig.5 it can be seen that a well defined value for T_g can be obtained from these fits for most values of implantation energy, however at the shallowest implantation level of 0.5 keV the overall value of ν and its T dependence are both significantly suppressed, preventing an accurate estimation of T_g from ν alone. In this case we estimate T_g from a combined fit of ν and the asymmetry a_D , whose T dependence also exhibits a slope change at T_g (Fig.5d).

The parameters obtained from single component analysis of the data via Eqn.1 are shown in Fig.6a-e and the corresponding parameters for two component analysis of Eqn.3 are shown in Fig.6f-j. The dependence of T_g on the mean implantation depth below the free surface is very similar for both analysis methods and shows significant suppression with respect to the bulk value for depths of 20 nm and below. The fractional suppression of T_g at the surface is of order 20%, which is comparable with that seen in our other LEM studies of PS [10] and PB [15], as well as matching the reduction found at a free polymer surface in molecular dynamics simulations [23].

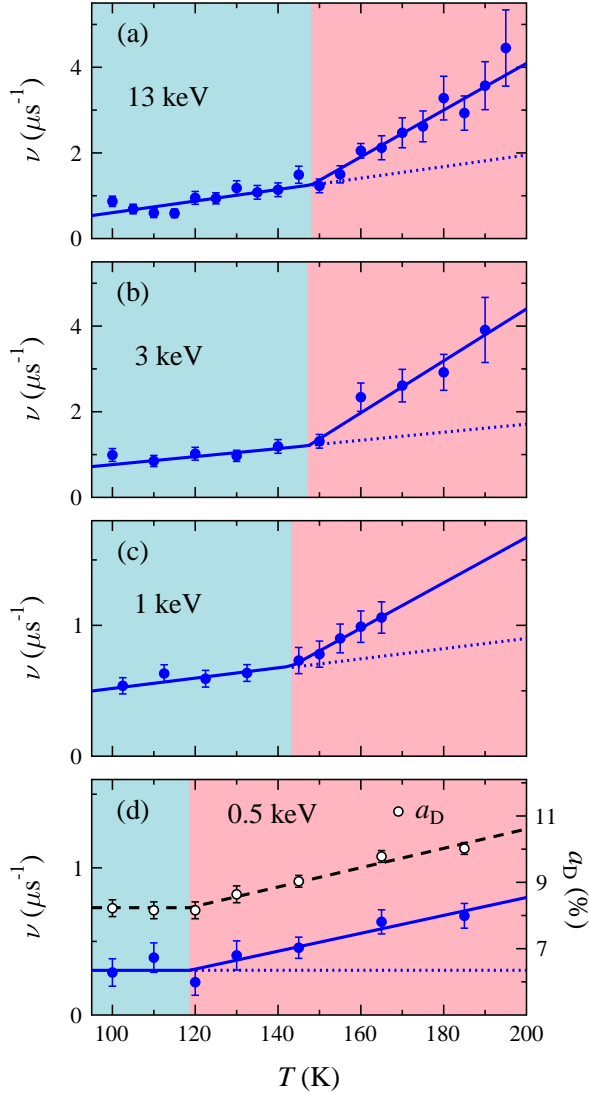


Fig. 5. (a)-(d) show the temperature dependent fluctuation rate of the local field seen by diamagnetic muons in a thin film sample of PDMS ($M_w=98$ kDa) in a transverse field of 10 mT at different muon implantation energies fitted to Eqn.1. The glass transition is seen as a change in the slope of the fluctuation rate versus temperature and the solid lines show fits to Eqn.5. For 0.5 keV implantation the ν values are significantly suppressed and an accurate estimation of T_g requires simultaneous fitting to the T dependence of both ν and the diamagnetic asymmetry a_D .

The length scale for this surface T_g suppression is comparable to the random coil end-to-end distance R_{EE} for this molecular weight of polymer.

There is a significant increase in σ as the implantation energy is reduced and the free surface is approached for the single component fit (Fig.6d). This is attributed to the reflection of muons in the low-

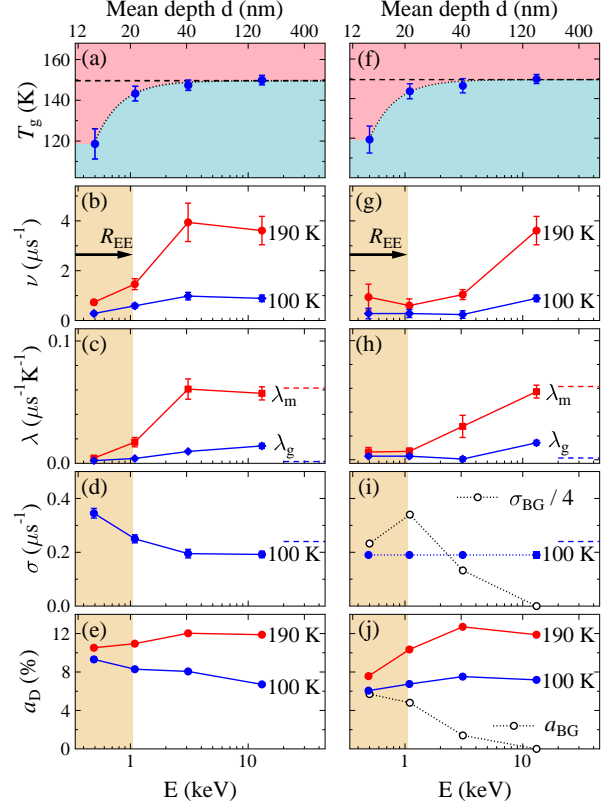


Fig. 6. (a) to (e) show parameters for the PDMS data of Fig.5 plotted against implantation energy with the corresponding mean implantation depth indicated on the upper scale. The shaded area in panels (b) to (e) indicates R_{EE} , the mean end-to-end distance of the polymer chains. Dashed lines indicate parameter values obtained for measurements on a bulk sample. Panels (f) to (j) show the corresponding results from the two component analysis described in the text, where the sample parameter σ is taken to be independent of depth.

energy tail of the energy spectrum that stop in the radiation shield, where they see a different magnetic field from those stopping in the sample, causing the increase in signal broadening. The two component fit compensates for this background component. Near the surface there is also a general suppression of ν (Fig.6b,g) and the slopes λ_m and λ_g (Fig.6c,h). In the background corrected analysis the width of the region where this suppression occurs is found to extend up to 40 nm (Fig.6g,h). The corresponding diamagnetic asymmetry in the sample is also plotted in Fig.6j for two temperatures. It is found to be dependent on both implantation energy and T , reflecting a shifting balance between the final fractions of paramagnetic and diamagnetic muon probe states.

To gain some insight into the general factors affecting ν and its T dependent slopes some TF μ SR

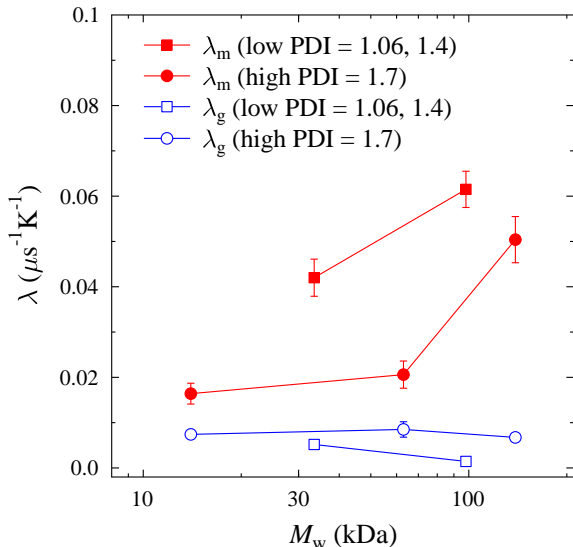


Fig. 7. The slope $\lambda = d\nu/dT$ as a function of molecular weight and polydispersity index for bulk samples of PDMS. The value λ_m is for the melt region $T > T_g$ and the value λ_g is for the glass region $T < T_g$.

measurements were made on bulk PDMS samples of varying M_w and PDI. The results of these measurements are shown in Fig.7. The data are grouped into low PDI and high PDI samples originating from the different sample suppliers. For both the low and high PDI samples the λ_m values increase significantly at high M_w . In the high PDI samples λ_g is larger than in the low PDI set, whereas λ_m is larger for the low PDI samples. Therefore the best contrast between λ_m and λ_g is seen for low PDI samples with high M_w . These trends presumably reflect changes in the way that dipolar field averaging dynamics that is seen by the muon is being coupled to the α structural relaxation process of the glass-liquid transition, but the details are not clear at present.

A key issue to be considered is the origin of the intrinsic suppression of ν and λ_m in the depth region nearest to the surface, an apparently universal effect that has been observed in every film sample we have studied using LEM in TF mode. It is at first sight surprising to find a reduction in the fluctuation rate of the dipolar field in the near-surface region where the suppression of the glass transition suggests a significantly faster overall dynamics. This feature may however be understood as being the result of strong anisotropy of the polymer dynamics near the surface. In particular the presence of the surface imposes confinement of the chain motion perpendicular to the surface, whereas for a free surface the mo-

tion parallel to the surface has less constraints than in the bulk. Such dynamical anisotropy at a free polymer surface has recently been observed experimentally in the diffusion of nanoparticles embedded in a PS film [24] where in-plane diffusion was found to be many orders of magnitude faster than out-of-plane diffusion. The faster motion parallel to the surface outweighs the suppression of the perpendicular motion resulting in the overall depression of T_g near the surface. Our measurements here with the magnetic field perpendicular to the surface produce a greater sensitivity to local motion in the out of plane direction. This is because such motion provides a more efficient averaging of the dipolar field width of the muon spin rotation signal compared to local motion in directions parallel to the plane. The present results suggest that making further LEM measurements comparing between data with the field oriented parallel and perpendicular to the plane of the film could be a useful way to study the evolution of the anisotropy of the dynamics versus depth below the free surface.

4.2. Data for PB

Complementary studies of the suppression of T_g in PB films in the region near the free surface using LEM and its dependence on M_w are being reported elsewhere [15]. Here we focus on the LEM data obtained for such PB samples in a relatively deep implantation region located beyond the near-surface region at depths of around 100 to 250 nm. The data for ν versus T are shown in Fig.8a. For implantation at 6.6 keV and below there is only a single transition, as also seen in bulk, whereas for implantation between 11.4 and 23 keV a dramatic feature of the data is the broadening of the transition region that can be represented by two separate and distinct transition temperatures T_g^L and T_g^H . In this case $\nu(T) - \nu_0$ is taken to follow three T linear regions defined by

$$\lambda_g T \quad : \quad T < T_g^L \quad (6)$$

$$\lambda_g T_g^L + \lambda_i (T - T_g^L) \quad : \quad T_g^L < T < T_g^H,$$

$$\lambda_g T_g^L + \lambda_i (T_g^H - T_g^L) + \lambda_m (T - T_g^H) \quad : \quad T > T_g^H.$$

The splitting $T_g^H - T_g^L$ reaches a maximum at a depth of around 175 nm (Fig.8b). At this depth T_g^L corresponds to the suppressed T_g value found at the free surface of the polymer [15], whereas T_g^H is some 20 K above the bulk T_g .

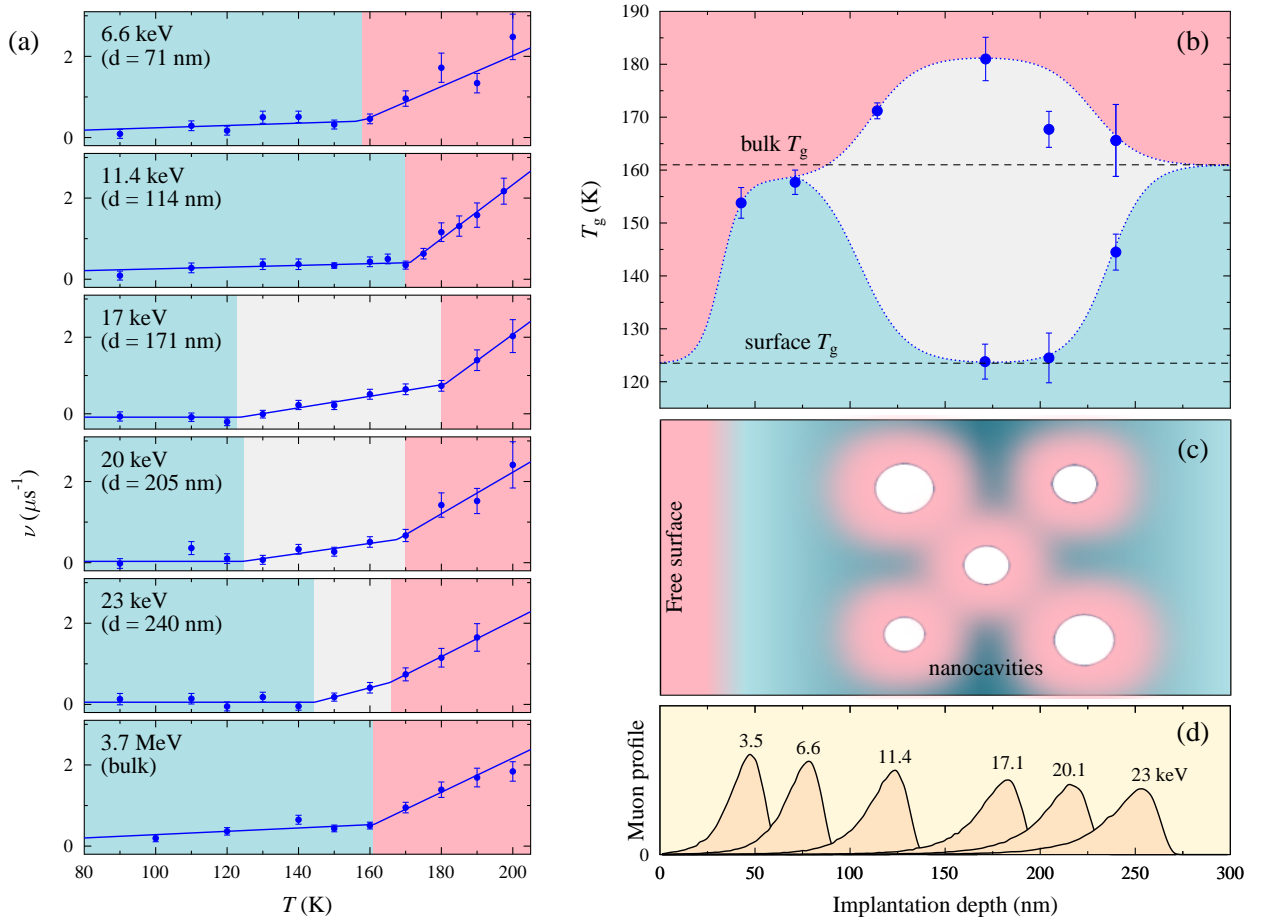


Fig. 8. (a) T -dependent fluctuation rate for a PB film where the muons are stopping significantly below the free surface of the polymer. The bottom panel shows measurements on the bulk polymer for comparison with the film data. For the energies 17, 20 and 23 keV there are two distinct transitions that straddle the bulk transition temperature. (b) shows corresponding local T_g values against implantation depth. Dotted lines and extrapolated shading are a guide to the eye. A model for the internal structure of the sample that is consistent with the observed data is shown as a schematic sectional map in (c), whose key feature is a buried region of nanocavities, with the interior cavity surfaces having T_g suppressed to the value found independently at the free surface [15] (suppressed T_g regions are shown in pink). Material locally displaced by cavity formation has above average density and hence local T_g above the bulk value. Muon stopping profiles are shown in (d).

The most straightforward interpretation of these results is that we have a region in the sample at a depth of around 200 nm that contains nanoscale structure in the form of nanocavities of some form, e.g. nanopores or nanobubbles. (Fig.8c). Nanobubbles at surfaces and interfaces have been studied for several years, but less is known about nanobubbles or nanopores at depths below the immediate surface region [25]. The nanocavities in our sample are likely to take the form of nanopores that are produced as the solvent streams and evaporates during the spin-casting process. The region around the surface of each cavity has a depressed T_g exactly matching that found at the free surface of the film

[15], thus explaining the sample fraction showing low T_g . The high T_g sample fraction is believed to result from local compression of the material in between the cavities as the cavity is formed, leading to a higher density than average and thus a T_g value enhanced over bulk. We note that an enhancement of T_g by $\sim 10\%$ has also been observed in nanostructured poly(methyl methacrylate) (PMMA) [26], which is comparable with the enhancement factor observed in our data. There was no evidence in that study for any second reduced T_g phase [26], but the surface effect in PMMA is known to be more complicated than in PS [4], with its sign dependent on tacticity [27], leading to significant reduction of the

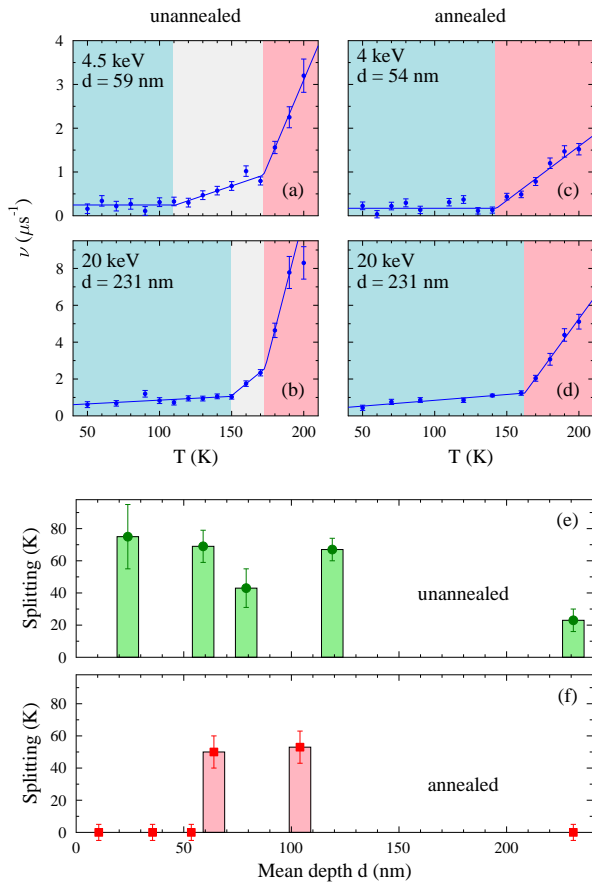


Fig. 9. (a) and (b) show fluctuation rate data for an unannealed PB sample ($M_w = 94$ kDa) at two different implantation energies which show a splitting of the glass transition. (c) and (d) show data for a sample prepared with exactly the same spin coating procedure but subjected to additional thermal annealing in order to reduce the sub-surface nanoscale inhomogeneity. This reduces the thermal behaviour to a single transition, but also notably reduces the slope $d\nu/dT$ in the region above T_g . (e,f) show the effect of annealing on the $T_g^H - T_g^L$ splitting at a range of implantation depths. The depth range of the spatial region retaining nanoscale inhomogeneity is seen to be considerably reduced by annealing and the average splitting in the remaining region is also reduced.

size of the effect in typical non-isotactic samples via cancellation of opposite contributions.

The well defined layer in which we observe the nanobubbles can be understood as resulting from two competing effects, firstly the bubbles rise towards the free top surface producing a greater density of bubbles there, but then very close to the free surface the solvent is able to be released by evaporating from the free surface and the bubbles are destroyed in the topmost layer. Since the buried nanos-

structure observed in the PB sample was believed to be the result of these inhomogeneities formed during the spin casting process, a set of experiments were carried out to test whether a period of thermal annealing could reduce or remove the nanostructured buried region found in the sample. For this purpose two identical samples were prepared, one was left without annealing and the other was annealed for 6 h at 343 K. The LEM results for these two samples are compared in Fig.9. At both low and high implantation depths there is a dramatic change in the T dependence of ν , as illustrated in Fig.9a-d, where the splitting is completely removed by the annealing. Studies over a wider range of implantation depths show that the region of splitting is still present, but the range of depths over which it remains has been significantly reduced (Fig.9f) in comparison with the range of depths found in the unannealed sample (Fig.9e).

It can also be seen from comparing Figs.9a-d that there is also a significant reduction of the slope λ_m for the melt phase of the annealed samples, suggesting that following the annealing process the polymer chains are becoming less able to reorient themselves with respect to the out of plane field axis, perhaps as a result of becoming more closely aligned with the plane of the sample and undergoing a greater confinement of motion along the field axis.

5. Discussion and Conclusion

Using the LEM technique the surface suppression of T_g has now been seen for the three different polymers PS, PDMS and PB. The level of suppression is of order 20% of the bulk T_g in each case. For PB a length scale for the mobile layer depth that increases with M_w is very clearly seen and the details are being reported elsewhere[15]. Simulating the generic surface behaviour of glasses with a coarse grained model has had some recent success in describing the dependence of T_g in polymer films of varying thickness [28], however describing the M_w dependence that is unique to polymer glasses require another modelling approach [29] that is based on the model of de Gennes[5] for transmission of mobility from the surface into the bulk of the film via conformational fluctuations propagating along the polymer chains[15].

Something that is clear from the present results is that the single dynamical parameter ν and its corresponding T derivatives λ_m and λ_g that we extract

from our data is dependent on many contributing mechanisms and is coupled to the glass dynamics in a correspondingly complex way. One result of this is that we are unable to simply identify the extent of the mobile layer at fixed T by just observing the dependence of ν on implantation depth. This is because the fall in ν on going from the mobile region to the glass region is overwhelmed by the large overall increase in ν that occurs on moving away from the surface region and this increase takes place both above and below the bulk T_g . Fortunately however the glass transition is revealed very clearly in the T scans that are made at fixed implantation depth.

It will be important to try and understand the general suppression of ν as the surface is approached in order to better interpret what is happening with the glass transition near the surface. In this respect enhancement of the anisotropic character of the dynamics near the surface seems to be the most likely origin. In this work we have established some of the factors determining the T dependence of ν both above and below T_g . Further understanding requires additional LEM experiments aimed at measuring the dynamical anisotropy. Carrying out detailed simulation work on the effect of different types of polymer motion on the muon spin relaxation may also be the key to developing analysis methods beyond the basic Arrhenius function. Sophisticated analysis methods of this type may be able to extract more detailed dynamical information from the muon data than is possible at present.

The present results demonstrate some of the unique capabilities of the LEM technique for studying local changes in polymer dynamics taking place near a free surface and show that LEM provides a promising new method for studying surface-modified local dynamics of polymers, as well as providing a novel technique for revealing buried nanostructured regions in polymer films. In the decade since the first LEM studies of a polymer surface were made in 2005[10] the capabilities of the PSI-LEM instrument have significantly improved, with data rates being enhanced following the construction of a new beamline. Recently a spin rotator has been installed that allows both TF and LF studies to be made. This gives access to both diamagnetic and paramagnetic muons as probe states, each offering quite different probe characteristics. Although the LF option was not available for the period when the present measurements were taken, the LF configuration offers great potential for future LEM studies to gain more detailed information on

the distribution of relaxation times. Such LF studies require a significant paramagnetic fraction to be present, which may not be satisfied for all polymers, whereas a diamagnetic fraction is always present so that the TF method is always available in principle, although thermally activated muon diffusion may prevent the TF method from being so useful for polymers with higher values of T_g , as was recently found for PS [13]. Besides the improved capabilities of the PSI-LEM instrument located in Switzerland, another ultra slow muon facility is currently being built at the J-PARC Center in Japan. The addition of a second user instrument capable of carrying out this type of LEM polymer study should provide a significant boost to the future possibilities in this area of research.

The authors thank V. Chan for sample preparation and H. Luetkens and R. Scheuermann for assistance with measurements using GPS and DOLLY. The experimental work was mainly carried out at the Swiss Muon Source $S\mu S$. TL was supported by the UK EPSRC. The LEM polymer dynamics project has received funding from the European Union's Seventh Framework Programme for research, technological development and demonstration under the NMI3-II Grant number 283883.

References

- [1] J. L. Keddie, R. A. L. Jones, R. A. Cory, Size-dependent depression of the glass transition temperature in polymer films. *Europhys. Lett.* 27 (1994) 59.
- [2] J. A. Forrest, K. Dalnoki-Veress, The glass transition in thin polymer films. *Adv. Coll. Int. Sci.* 94 (2001) 167.
- [3] C. J. Ellison, J. M. Torkelson, The distribution of glass-transition temperatures in nanoscopically confined glass formers. *Nature Mater.* 2 (2003) 695.
- [4] M. Alcoutlabi, G. B. McKenna, Effects of confinement on material behaviour at the nanometre size scale. *J.Phys.: Condens. Matter* 17 (2005) R461.
- [5] P.G. de Gennes, Glass transitions in thin polymer films, *Eur. Phys. J. E: Soft Matter Biol. Phys.* 2 (2000) 201.
- [6] E. Morenzoni, in: S.L. Lee, S.H. Kilcoyne and R. Cywinski (eds.), *Muon Science*, IOP Publishing, Bristol and Philadelphia (1999) p343.
- [7] P. Bakule, E. Morenzoni, Generation and applications of slow polarized muons, *Contemp. Phys.* 45 (2004) 203.
- [8] E. Morenzoni, T. Prokscha, A. Suter *et al*, Nano-scale thin film investigations with slow polarized muons, *Journal of Physics: Condensed Matter*, 16 (2004) S4583.
- [9] T. Prokscha, E. Morenzoni, K. Deiters *et al*, The new E4 beam at PSI: a hybrid-type large acceptance channel for the generation of a high intensity surface-muon beam, *Nucl. Instr. Meth. A* 595 (2008) 317.

- [10] F. L. Pratt, T. Lancaster, M.L. Brooks *et al*, Surface dynamics of a thin polystyrene film probed by low-energy muons. Phys. Rev. B 72 (2005) 121401(R).
- [11] F.L. Pratt, S.J. Blundell, T. Jestaedt *et al*, μ SR of conducting and non-conducting polymers, Physica B 289-290 (2000) 625.
- [12] F.L. Pratt, S.J. Blundell, I.M. Marshall *et al*, μ SR in polymers, Physica B 326 (2003) 34.
- [13] T. Kanaya, H. Ogawa, M. Kishimoto *et al*, Distribution of glass transition temperatures T_g in polystyrene thin films as revealed by low-energy muon spin relaxation: A comparison with neutron reflectivity results, Phys. Rev. E92 (2015) 022604.
- [14] R. Inoue, K. Kawashima, K. Matsui *et al*, Distributions of glass-transition temperature and thermal expansivity in multilayered polystyrene thin films studied by neutron reflectivity, Phys. Rev. E 83 (2011) 021801.
- [15] F.L. Pratt, T. Lancaster, P.J. Baker *et al*, Depth-resolved glass transition near a polymer surface (in preparation).
- [16] W. Eckstein, Computer Simulation of Ion-Solid Interactions, Springer-Verlag, Berlin, 1991.
- [17] E. Morenzoni, H. Glucker, T. Prokscha *et al*, Implantation studies of keV positive muons in thin metallic layers, Nucl. Instr. Meth. B192 (2002) 254.
- [18] F. L. Pratt, WIMDA: a muon data analysis program for the Windows PC, Physica B 289-290 (2000) 710.
- [19] A. Abragam, Principles of Nuclear Magnetism, Oxford University Press, Oxford, 1961.
- [20] F.L. Pratt, Repolarisation of anisotropic muonium in orientationally disordered solids, Philosophical Magazine Letters 75 (1997) 371.
- [21] F.L. Pratt (unpublished).
- [22] Gaussian 09, Revision D.01, M. J. Frisch, G. W. Trucks, H. B. Schlegel *et al*, Gaussian, Inc., Wallingford CT, 2013.
- [23] J.A. Torres, P.F. Nealey and J.J. de Pablo, Phys. Rev. Lett. 85 (2000) 3221.
- [24] N. Begam, S. Chandran, N. Biswas and J.K. Basu, Soft Matter 11 (2015) 1165.
- [25] J. R. T. Seddon, D. Lohse, W.A. Ducker, V.S.J. Craig, A deliberation on nanobubbles at surfaces and in bulk, ChemPhysChem 13 (2012) 2179.
- [26] Y. Guo, A. Morozov, D. Schneider *et al*, Ultrastable nanostructured polymer glasses. Nature Mater. 11 (2012) 337.
- [27] Y. Grohens, L. Hamon, G. Reiter *et al*, Some relevant parameters affecting the glass transition of supported ultra-thin polymer films. Eur. Phys. J. E 8 (2002) 217.
- [28] J. DeFelice, S.T. Milner, J.E.G. Lipson, Simulating local T_g reporting layers in glassy thin films, Macromol. 49 (2016) 1822.
- [29] S.T. Milner, J.E.G. Lipson, Delayed glassification model for free-surface suppression of T_g in polymer glasses, Macromol. 43 (2010) 9865.